Complex Formation between NADH Model Compounds and Metalloporphyrins

Shunichi Fukuzumi,* Yuji Kondo, Seiji Mochizuki, and Toshio Tanaka†
Department of Applied Chemistry, Faculty of Engineering, Osaka University, Suita, Osaka 565, Japan

Various NADH model compounds, 1-(X-benzyl)-1,4-dihydronicotinamide (X-BNAH: X = 4-MeO, 4-Me, H, 4-Cl_2, and 2,4-Cl_2) and 10-methyl-9,10-dihydroacridine ($AcrH_2$), form complexes with metalloporphyrins ($FeTPPClO_4$, FeTPPCl, $MnTPPClO_4$, and ZnTPP; TPP: tetraphenylporphyrin) in dichloromethane or chloroform. For the BNAH–ZnTPP system, the stoicheiometry of the complex formation is 1:1 with the formation constant K = 50 dm^3 mol^{-1} in dichloromethane at 298 K. In the BNAH–$MTPPClO_4$ system (M = Fe and Mn), both 1:1 and 2:1 complexes are formed depending on the ratio of BNAH to $MTPPClO_4$. The formation constant becomes larger as the donor ability of NADH model compounds increases. Both the five-co-ordinate $FeTPP(BNAH)^+$ and six-co-ordinate $FeTPP(BNAH)_2^+$ complexes are high-spin (S = 5/2) species. The complex formation between the reduced metalloporphyrin (FeTPP and MnTPP) with BNAH was also investigated by the technique of cyclic voltammetry, which revealed that the reduced iron porphyrin FeTPP also forms a bis-co-ordination complex with BNAH, but the MnTPP forms only a mono-ligand adduct with BNAH. NADH model compounds are shown to act as two-electron donors in the electron-transfer reactions with $FeTPPClO_4$ in the presence of oxygen in acetonitrile, when the overall rates are determined by the rates of electron transfer from X-BNAH to $FeTPP^+$ together with the competition between the back electron transfer from FeTPP to X-$BNAH^{+\bullet}$ and the deprotonation of $BNAH^{+\bullet}$.

Reduced nicotinamide adenine dinucleotide (NADH) is known to act as a two-electron donor in the respiratory chain, where electrons are transferred from NADH to dioxygen through a chain of metalloenzymes which contain iron complexes.[1,2] Two electrons required for mono-oxygenation of substrates, catalysed by cytochrome P-450 which contains iron porphyrins in the active site, are also provided by NADH through mediators such as flavoprotein (adrenodoxin reductase) and iron–sulphur protein (adrenodoxin).[3] NADH can also reduce carbonyl compounds by the transfer of a hydride ion (equivalent to two electrons and a proton) in the presence of liver alcohol dehydrogenase which contains a zinc complex in the active site.[4] Thus, iron and zinc complexes play an essential role in biological redox reactions where NADH is used as a two-electron source. In this context, the interaction between NADH model compounds and metal complexes have been extensively studied.[5] However, no study of the interaction between NADH model compounds and metalloporphyrins has so far been reported, in spite of extensive studies on the co-ordination of a variety of abiological ligands to metal porphyrins.[6–8]

In this study, we report that metal porphyrins (ZnTPP, $FeTPPClO_4$, FeTPPCl, $MnTPPClO_4$, and $CoTPPClO_4$) with no axial metal bound ligands can form complexes with NADH model compounds (1-benzyl-1,4-dihydronicotinamide derivatives and 10-methyl-9,10-dihydroacridine) in dichloromethane or chloroform.[9] The properties of the metal porphyrin complexes with NADH model compounds are examined by spectroscopic (u.v.–visible, ^1H n.m.r., and e.s.r. spectroscopy) and electrochemical methods. Electron-transfer reactions from NADH model compounds to $FeTPPClO_4$ in the presence of oxygen in MeCN are also reported.

Experimental

Materials.—Preparations of 1-(X-benzyl)-1,4-dihydronicotinamide (X-BNAH: X = 4-MeO, 4-Me, H, 4-Cl, and 2,4-Cl_2), [4-^{2}H]-1-benzyl-1,4-dihydronicotinamide ([4-^{2}H]-BNAH), and 10-methyl-9,10-dihydroacridine ($AcrH_2$), used as

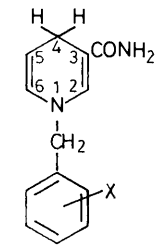

(X-BNAH)

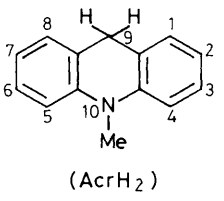

($AcrH_2$)

NADH model compounds, were described previously.[10,11] 1-Benzylnicotinamide perchlorate ($BNAClO_4$) was prepared by the addition of $NaClO_4$ to BNACl in water. Tetraphenylporphirinatoiron(III) chloride ($FeTPPCl$)[12] and zinc(II) tetraphenylporphyrin (ZnTPP)[13] were synthesized and purified according to the literature. Cobalt(II) tetraphenylporphyrin (CoTPP) was prepared according to the literature method,[14] and oxidized by oxygen in the presence of HCl in methanol to obtain tetraphenylporphyrinatocobalt(III) chloride ($CoTPPCl$) which was purified by recrystallization from methanol.[15] The perchlorate salts of $FeTPP^+$, $MnTPP^+$, and $CoTPP^+$ were prepared from the corresponding chloride salts by reaction with $AgClO_4$ and recrystallized from toluene.[16] The μ-oxo-dimer $(FeTPP)_2O$ was prepared by the reaction of $FeTPPClO_4$ with the radical anion salt of 2,3,4,6-tetrachloro-1,4-benzoquinone in the presence of oxygen in acetonitrile. The purity of the metalloporphyrins was checked by elementary analyses which gave satisfactory results. Zinc perchlorate ($ZnClO_4 \cdot 6H_2O$) was obtained commercially and purified by a standard method. Reagent grade MeCN was purified by the successive distillation (four times) over P_2O_5 before use. Spectroscopic grade dichloromethane and chloroform were obtained from Wako Pure Chemicals and used without further purification.

† *Current address:* Department of Applied Physics and Chemistry, Fukui Institute of Technology, Fukui 910, Japan.

Table 1. Formation constants K_1 and K_2 for the complexes formed between metalloporphyrins ($FeTPPClO_4$, FeTPPCl, $MnTPPClO_4$, $CoTPPClO_4$, and ZnTPP) and NADH model compounds in CH_2Cl_2 at 298 K, and the one-electron oxidation potentials of NADH model compounds in MeCN at 298 K.

Metallo-porphyrin	Ligand	E^0_{ox} *vs.* *SCE*[a]/V	K_1[b]/ $dm^3\ mol^{-1}$	K_2[b]/ $dm^3\ mol^{-1}$
$FeTPPClO_4$	4-MeOBNAH	0.50	1.6×10^4	7.6×10^2
$FeTPPClO_4$	4-MeBNAH	0.54	9.3×10^3	7.0×10^2
$FeTPPClO_4$	BNAH	0.57	7.9×10^3	6.7×10^2
$FeTPPClO_4$	4-ClBNAH	0.62	5.4×10^3	3.6×10^2
$FeTPPClO_4$	2,4-Cl_2BNAH	0.59	4.9×10^3	2.3×10^2
$FeTPPClO_4$	$AcrH_2$	0.80	2.1×10^3	2.4×10^2
FeTPPCl	BNAH	0.57	2.6×10	—
$MnTPPClO_4$	BNAH	0.57	2.5×10^2	8.5×10
$CoTPPClO_4$	BNAH	0.57	*c*	*c*
ZnTPP	BNAH	0.57	5.0×10	*c*

[a] Taken from ref. 10. [b] The experimental errors are within ±10%. [c] Too small to be determined accurately.

Spectroscopic Measurements.—Electronic absorption spectra were measured using a Union SM-401 spectrophotometer with a quartz cell which was placed in a thermostatted compartment at 298 K. Kinetic measurements were performed using a Union RA-103 stopped flow spectrophotometer under a four times atmospheric pressure of oxygen at 298 K. Rates of the reactions of $FeTPPClO_4$ with NADH model compounds in the presence of oxygen were monitored by the rise and decay of absorption bands at 570 and 530 nm for the formation of $(FeTPP)_2O$,[17] and the disappearance of $FeTPPClO_4$, respectively. The concentrations of NADH model compounds were chosen as being in more than tenfold excess of $FeTPPClO_4$ to maintain the pseudo-first-order conditions. The pseudo-first-order rate constants (k_{obs}) were determined by least-squares curve fitting using Union System 77 microcomputer.

^1H N.m.r. spectra were recorded on a JEOL-PS-100 spectrometer. Downfield chemical shifts (ppm) are given as positive sign referenced to $SiMe_4$. The Evans n.m.r. method[18] was applied to determine the solution magnetic susceptibilities of paramagnetic complexes of $FeTPPClO_4$ with BNAH. A capillary tube containing the solvent (CD_2Cl_2) and the same concentration of BNAH was inserted in the n.m.r. tube, which contains a CD_2Cl_2 solution of BNAH (0.02 or 0.04 mol dm^{-3}) and $FeTPPClO_4$ (0.02 mol dm^{-3}). A diamagnetic correction for the TPP ligand was made based on the reported value.[19] The change of solvent density with temperature was also taken into account in the determination of the solution magnetic susceptibilities.[20]

E.s.r. spectra were measured with a JEOL X-band spectrometer (JES-ME-2X) at 77 K. The *g*-values of the e.s.r. spectra were calibrated by using an Mn^{2+} e.s.r. marker.

Oxidation of BNAH *by* $FeTPPClO_4$.—In a typical reaction, BNAH (65 μmol) was added to an air-saturated MeCN solution containing $FeTPPClO_4$ (128 μmol) at 298 K. The μ-oxo dimer $(FeTPP)_2O$ (64 μmol) was formed and identified by its characteristic visible spectrum in MeCN.[17] The addition of H_2O to the reaction mixture resulted in the precipitation of $(FeTPP)_2O$ which was removed by filtration. Then, the amount of proton (60 μmol) formed in the reaction was determined by pH measurement of the filtrate; the pH of the filtrate aqueous solution (50 cm^3) was 2.92. On removal of H_2O by evaporation, the two-electron oxidation product, $BNAClO_4$ (60 μmol), was isolated and identified from its ^1H n.m.r. spectrum in CD_3CN. The same procedure was performed for the oxidation of [4-^2H]BNAH by $FeTPPClO_4$, and the deuterium isotope effect ($Y_H/Y_D = 1.7 \pm 0.2$) was determined from the ratio of BNA^+ to [^2H]BNA^+ using ^1H n.m.r. spectroscopy.

Cyclic Voltammetry.—Cyclic voltammetric measurements were carried out with a Hokuto Denko Model HA-104 or 301 potentiostat/galvanostat, using the three-electrode system with platinum working and counter electrodes and a saturated calomel reference electrode (SCE). The experiments were carried out in CH_2Cl_2 containing 0.1 mol dm^{-3} NBu_4ClO_4, as a supporting electrolyte, at 293 K. The sweep rates were varied in the 20–250 mV s^{-1} range. The cyclic voltammograms of $FeTPPClO_4$ and $MnTPPClO_4$ in the absence and presence of BNAH exhibited quasi-reversible cathodic and anodic peaks for the Fe^{III}/Fe^{II} and Mn^{III}/Mn^{II} couples, respectively. The minimum peak separation (70 mV) obtained at the slow sweep rate (20 mV s^{-1}) was close to the Nernstian value.

Results and Discussion

Complex Formation between NADH *Model Compounds and Iron*(III) *Porphyrins.*—Addition of BNAH (λ_{max} 350 nm) to a CH_2Cl_2 solution of $FeTPPClO_4$ results in a significant change of the visible spectrum as shown in Figure 1. An isosbestic point is observed at 410 nm at low concentrations of BNAH [Figure 1(*a*)]. However, crossover points at 510, 553, and 660 nm observed at the low BNAH concentrations spread over slightly in a progressive manner when the BNAH concentration was increased and then, new isosbestic points are observed at 504, 552, and 652 nm at the higher BNAH concentrations [Figure 1(*b*)]. Such spectroscopic changes may be interpreted as being due to the formation of complexes between $FeTPPClO_4$ and BNAH, where (BNAH) axially co-ordinating to $FeTPPClO_4$ requires two steps. The first step is the formation of a 1:1 complex [equation (1)] and the second step is an

$$FeTPP^+ + BNAH \overset{K_1}{\rightleftharpoons} FeTPP(BNAH)^+ \quad (1)$$

additional axial ligand addition to form a 1:2 complex [equation (2)]. Thus, the absorption maxima of $FeTPPClO_4$

$$FeTPP(BNAH)^+ + BNAH \overset{K_2}{\rightleftharpoons} FeTPP(BNAH)_2^+ \quad (2)$$

(λ_{max} 399, 528, and 664 nm) are changed to those of $FeTPP(BNAH)ClO_4$ (λ_{max} 417, 511, and 690 nm), and those of $FeTPP(BNAH)_2ClO_4$ (λ_{max} 417, 576, and 630sh nm) by an increase in the BNAH concentration (Figure 1). The addition of NBu_4ClO_4 (1.0×10^{-2} mol dm^{-3}) to the BNAH–$FeTPPClO_4$ system resulted in no appreciable change in the electronic spectra. Thus, there may be no competition for co-ordinating sites between the counter anion ClO_4^- and BNAH. Similar spectroscopic changes were observed on the addition of other NADH model compound (4-MeOBNAH, 4-MeBNAH, 4-ClBNAH, 2,4-Cl_2BNAH, and $AcrH_2$) to CH_2Cl_2 solutions of $FeTPPClO_4$.

The K_1 value in equation (1) may be calculated from equation (3), where $\alpha = (A - A_0)/(A_\infty - A_0)$; A is the absorbance at 417

$$(\alpha^{-1} - 1)^{-1} = K_1([BNAH]_0 - \alpha[FeTPP^+]_0) \quad (3)$$

nm in the presence of BNAH, A_0 and A_∞ are the initial and final absorbances at the same wavelength in the absence and presence of a large excess of BNAH such that all the BNAH molecules form the 1:1 complex, respectively. Typical examples

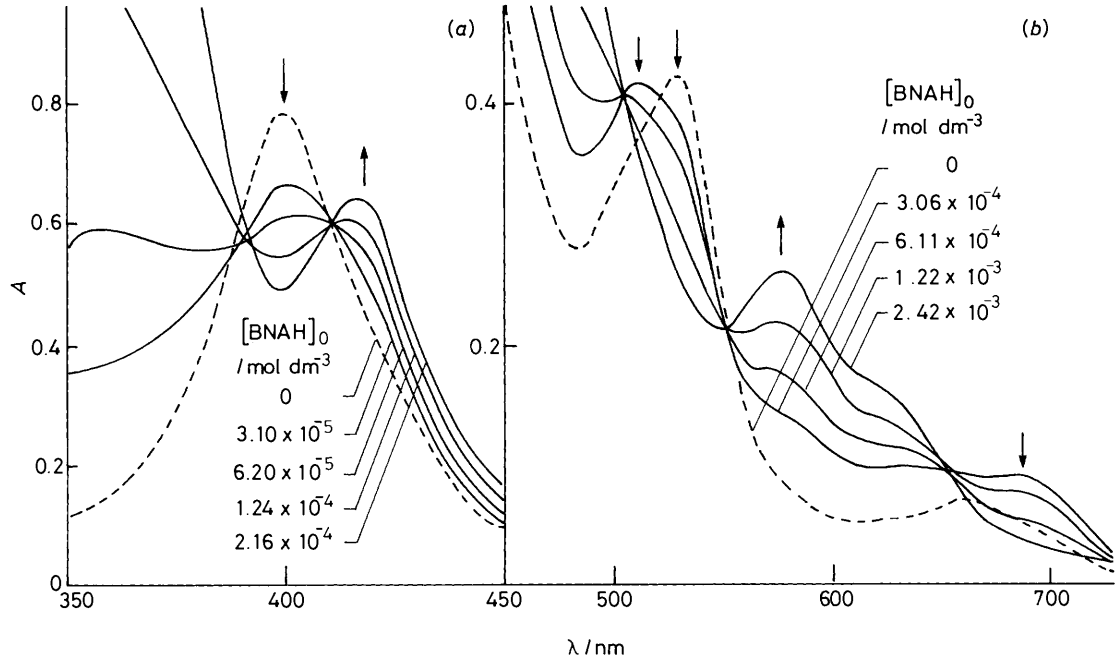

Figure 1. Visible spectroscopic change observed upon addition of BNAH to a CH_2Cl_2 solution of $FeTPPClO_4$; (*a*) 6.4 × 10^{-6} mol dm^{-3}, (*b*) 4.0 × 10^{-5} mol dm^{-3}.

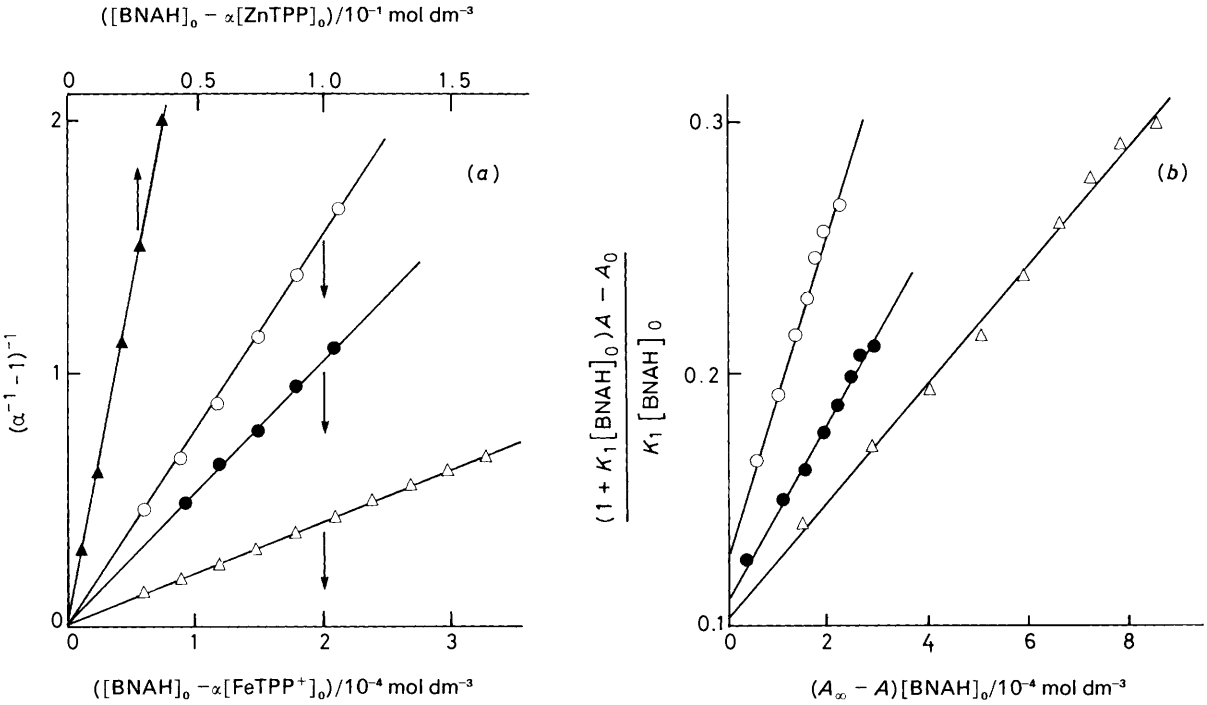

Figure 2. Plots for the determination of the stepwise formation constants (*a*) K_1 [equation (3)] and (*b*) K_2 [equation (5)] for the complexes formed between $FeTPPClO_4$ and NADH model compounds, BNAH (○), 4-ClBNAH (●), $AcrH_2$ (△), and for the complex formed between ZnTPP and BNAH (▲).

of the plots are shown in Figure 2(*a*), where good linear correlations are obtained. The K_1 values determined from the slopes of the plots are listed in Table 1.

The K_2 value in equation (2) can be determined by the use of the K_1 value as follows: the absorbance A at 576 nm which is the absorption maximum of the $FeTPP(BNAH)_2^+$ complex may be expressed by equation (4), where A_0 and A_1 are the absorbances due to $FeTPP^+$ in the absence of BNAH and due to $FeTPP(BNAH)^+$ in the presence of BNAH, respectively, and A_∞ is the absorbance due to $FeTPP(BNAH)_2^+$ in the presence of a large excess of BNAH such that all $FeTPP^+$ molecules form

$$A = \frac{A_0 + K_1[\mathrm{BNAH}]_0 A_1 + K_1K_2[\mathrm{BNAH}]_0^2 A_\infty}{1 + K_1[\mathrm{BNAH}]_0 + K_1K_2[\mathrm{BNAH}]_0^2} \quad (4)$$

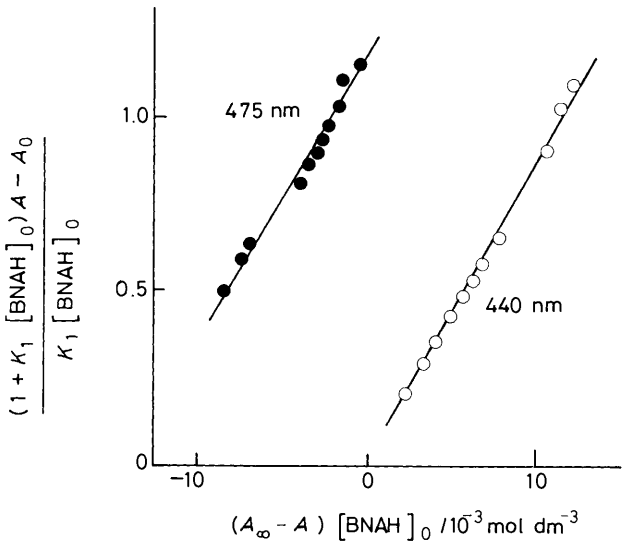

Figure 3. Plots for the determination of the K_1 and K_2 values for the complexes formed between $MnTPPClO_4$ and BNAH based on equation (5), see the text.

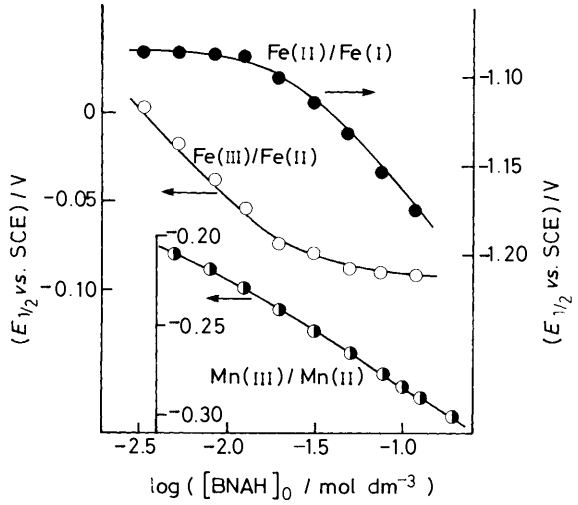

Figure 4. Plots of $E_{\frac{1}{2}}$ *vs.* log$[BNAH]_0$ for the reduction of $FeTPPClO_4$ (○), FeTPP (●), and $MnTPPClO_4$ (◑) in a CH_2Cl_2 solution containing various concentrations of BNAH at 298 K. The solid lines are drawn by the simulation based on equations (9) and (12), see the text.

the 1:2 complex with BNAH. Equation (4) can be rewritten as equation (5). Since the value of the left-hand side in equation (5)

$$\frac{(1 + K_2[BNAH]_0)A - A_0}{K_1[BNAH]_0} = K_2(A_\infty - A)[BNAH]_0 + A_1 \quad (5)$$

is obtained by using the K_1 value in Table 1, the K_2 value can be determined from the slope of a linear plot between the left-hand side in equation (6) and $(A_\infty - A)[BNAH]_0$. Typical examples of the plots are shown in Figure 2(*a*), where good linear correlations are observed in agreement with equation (5). The K_2 values thus obtained are also listed in Table 1, together with the one-electron oxidation potentials (E^0_{ox}) of the NADH model compounds in MeCN.[10] Both the K_1 and K_2 values increase with a negative shift in E^0_{ox}, when the donating ability and the basicity of NADH model compounds are increased.

Similar spectroscopic change was observed in the case of $MnTPPClO_4$ by the addition of BNAH, indicating the 1:1 and 2:1 complex formation between BNAH and $MnTPPClO_4$ [equations (6) and (7), respectively]. In this case, however, the

$$MnTPP^+ + BNAH \overset{K_1}{\rightleftharpoons} MnTPP(BNAH)^+ \quad (6)$$

$$MnTPP(BNAH)^+ + BNAH \overset{K_2}{\rightleftharpoons} MnTPP(BNAH)_2{}^+ \quad (7)$$

K_1 and K_2 values appear to be similar, and thus it is difficult to determine K_1 independently using equation (3). Then, the K_1 and K_2 values are determined simultaneously using equation (5), where A is taken as the absorbances at two different wavelengths (440 and 475 nm). The absorbances at these wavelengths exhibit different dependence on the BNAH concentration; the absorption maximum of $MnTPPClO_4$ at 475 nm increases with an increase in the BNAH concentration but decreases with a further increase in the BNAH concentration, when a new absorption maximum appears at 440 nm and its absorbance increases steadily with an increase in the BNAH concentration. Despite such differing behaviour of the absorbances at 440 and 475 nm, the plots of the left-hand side of equation (5) *vs.* $(A_\infty - A)[BNAH]_0$ at these two different wavelengths give a linear correlation which have the same slope, provided that an appropriate K_1 value is chosen, as shown in Figure 3. Since the linearity as well as the slope is sensitive to the K_1 value, a good estimate of the K_1 value (2.5×10^2 dm^3 mol^{-1}) can be obtained based on the plots in Figure 3, where the slope corresponds to the K_2 value, 85 dm^3 mol^{-1} (Table 1).

Addition of an NADH model compound (BNAH) to a CH_2Cl_2 solution containing ZnTPP also results in a change of the visible spectrum from λ_{max} 554 to 560 nm with an isosbestic point at 557 nm as observed in the formation of the monopyridinate of ZnTPP.[8,21,22] However, the change in the Soret absorption band at 416 nm in the presence of a large excess of BNAH was obscured by the overlap with the absorption band due to BNAH (λ_{max} 350 nm). The spectroscopic change may be ascribed to the complex formation between ZnTPP and BNAH with a 1:1 stoicheiometry, equation (8). In this case, however,

$$ZnTPP + BNAH \overset{K_1}{\rightleftharpoons} ZnTPP(BNAH) \quad (8)$$

no bis-co-ordination complex with BNAH was observed in the high concentration of BNAH (*e.g.*, 0.2 mol dm^{-3}). The K_1 value was determined as 50 dm^3 mol^{-1} (Table 1) from the plot of equation (3) in Figure 2(*a*) where A is the absorbance at 600 nm, and $[FeTPP^+]_0$ is replaced by $[ZnTPP]_0$. A somewhat smaller K_1 value was obtained in $CHCl_3$ (K_1 = 24 dm^3 mol^{-1}).

When $FeTPPClO_4$ is replaced by FeTPPCl in which the counter anion Cl^- is known to bind strongly to Fe, the K_1 value becomes much smaller and no 2:1 complex was formed between BNAH and FeTPPCl (Table 1). In the case of $CoTPPClO_4$, little change in the electronic spectrum was observed on addition of BNAH (Table 1).

Electrode Reactions of Metalloporphyrins in the Presence of NADH *Model Compounds.*—The electrode reactions of $FeTPP^+$ were investigated in CH_2Cl_2 containing various concentrations of BNAH by using cyclic voltammetry. The cyclic voltammograms of $FeTPPClO_4$ in the absence and presence of BNAH exhibited Nernstian separated cathodic and anodic peaks for the Fe^{III}/Fe^{II} and Fe^{II}/Fe^{I} couples, while the redox reaction of FeTPPCl for the Fe^{III}/Fe^{II} couple was irreversible as previously reported.[23] The half-wave potentials ($E_{\frac{1}{2}}$) of $FeTPPClO_4$ vary depending on the BNAH concentration as shown in Figure 4, where the $E_{\frac{1}{2}}$ values for the

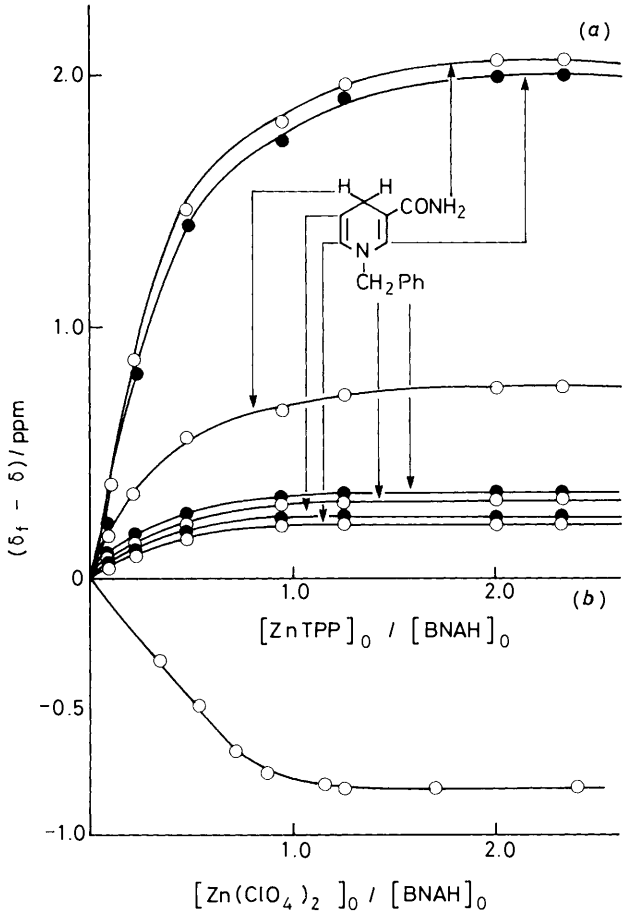

Figure 5. Plots of the changes in the chemical shifts of BNAH in the presence of (*a*) ZnTPP (2.9×10^{-2} mol dm^{-3}) and (*b*) $Zn(ClO_4)_2$ (3.0×10^{-2} mol dm^{-3}) relative to those in their absence ($\delta_f - \delta$) as a function of the ratios of the initial concentrations of ZnTPP and $Zn(ClO_4)_2$ to BNAH in $CDCl_3$ and $CDCl_3/CD_3CN$, respectively.

Fe^{III}/Fe^{II} and Fe^{II}/Fe^{I} couples are plotted as a function of log[BNAH]$_0$. In the low concentrations of BNAH ($< 10^{-2}$ mol dm^{-3}), the $E_{\frac{1}{2}}$ value for the Fe^{III}/Fe^{II} couple is shifted cathodically, when the $E_{\frac{1}{2}}$ value for the Fe^{II}/Fe^{I} couple is rather constant. Such a dependence of the redox potential on BNAH concentration is reversed in the high concentrations of BNAH ($> 10^{-2}$ mol dm^{-3}), where the $E_{\frac{1}{2}}$ value of the Fe^{III}/Fe^{II} couple is invariant, while the $E_{\frac{1}{2}}$ value of Fe^{II}/Fe^{I} couple is shifted cathodically. The Nernstian expression of $E_{\frac{1}{2}}$ for the Fe^{III}/Fe^{II} couple is given by equation (9), where K_1 and K_2 are the formation constants of

$$E_{\frac{1}{2}} = E^0(\text{FeTPP}^+/\text{FeTPP}) + \frac{2.3RT}{F} \log\left(\frac{1 + K'_1[\text{BNAH}]_0 + K'_1K'_2[\text{BNAH}]_0^2}{1 + K_1[\text{BNAH}]_0 + K_1K_2[\text{BNAH}]_0^2}\right) \quad (9)$$

$FeTPP(BNAH)^+$ and $FeTPP(BNAH)_2^+$, equations (1) and (2), respectively; K'_1 and K'_2 are the formation constants of FeTPP(BNAH) and $FeTPP(BNAH)_2$, equations (10) and (11),

$$\text{FeTPP} + \text{BNAH} \overset{K'_1}{\rightleftharpoons} \text{FeTPP(BNAH)} \quad (10)$$

$$\text{FeTPP(BNAH)} + \text{BNAH} \overset{K'_2}{\rightleftharpoons} \text{FeTPP(BNAH)}_2 \quad (11)$$

respectively. Similarly, the Nernstian expression of $E_{\frac{1}{2}}$ for the Fe^{II}/Fe^{I} couple is given by equation (12). Both the dependences

$$E_{\frac{1}{2}} = E^0(\text{FeTPP/FeTPP}^-) - (2.3RT/F)\log(1 + K'_1[\text{BNAH}]_0 + K'_1K'_2[\text{BNAH}]_0^2) \quad (12)$$

of $E_{\frac{1}{2}}$ for the Fe^{III}/Fe^{II} and Fe^{II}/Fe^{I} couples on [BNAH]$_0$ are well expressed by equations (9) and (12), respectively, as shown by the solid lines in Figure 4, where the K_1 and K_2 values are taken from Table 1, since they are unaffected by the presence of NBu_4ClO_4 as described above. The best fit value of $K'_1K'_2$ is obtained as 2.0×10^3 dm^6 mol^{-2}. The K'_1 value is too small to be determined accurately by the simulation based on equations (9) and (12). Thus, FeTPP also forms a bis co-ordination complex with BNAH [equation (11)], although the formation constant is much smaller than for $FeTPP^+$. The redox processes of $FeTPP^+$/FeTPP and their complex formation with BNAH are summarized in Scheme 1.

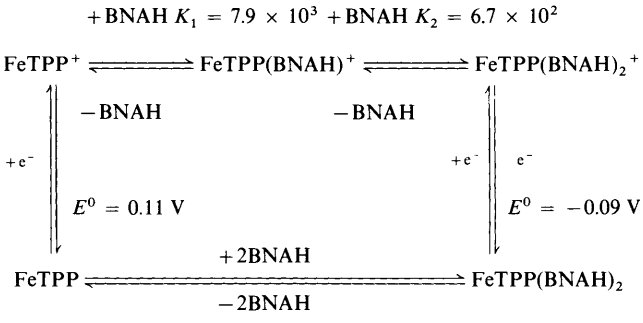

Scheme 1.

The $E_{\frac{1}{2}}$ value for the Mn^{III}/Mn^{II} couple exhibits a different dependence on [BNAH]$_0$ from that for the Fe^{III}/Fe^{II} couple as shown in Figure 4, where the $E_{\frac{1}{2}}$ value of Mn(III)/Mn(II) redox couple is shifted cathodically by 60 mV/log[BNAH]$_0$. Such a dependence of $E_{\frac{1}{2}}$ on [BNAH]$_0$ can also be expressed by equation (9) in which $FeTPP^+$ and FeTPP are replaced by $MnTPP^+$ and MnTPP, respectively. The best fit simulation curve is shown by the solid line in Figure 4, where the K_1 and K_2 values [equations (6) and (7), respectively] are also taken from Table 1 and the K'_1 value [equation (13)] is taken as 50 dm^3

$$\text{MnTPP} + \text{BNAH} \overset{K'_1}{\rightleftharpoons} \text{MnTPP(BNAH)} \quad (13)$$

mol^{-1}. In this case, the K'_2 value for the corresponding bis co-ordination complex is too small to be determined accurately by the simulation based on equation (9). Thus, unlike FeTPP, MnTPP forms only a mono-ligand adduct with BNAH. Such preferences of MnTPP and FeTPP to form mono- and bis co-ordination complexes, respectively, are well known for the corresponding pyridine complexes.[23,24] The redox processes of $MnTPP^+$/MnTPP and their complex formation with BNAH are summarized in Scheme 2.

Co-ordination Site of BNAH *in the* ZnTPP(BNAH) *Complex.*—The ^{1}H n.m.r. signals of BNAH in $CDCl_3$ exhibited large upfield shifts by the complex formation with ZnTPP. The observed chemical shifts referenced to free BNAH($\delta_f - \delta$) are shown as a function of the ratio of the initial concentration of ZnTPP to that of BNAH in Figure 5(*a*). What is observed is a weighted average of the chemical shifts of free BNAH and ZnTPP–BNAH complex depending on the ZnTPP to BNAH

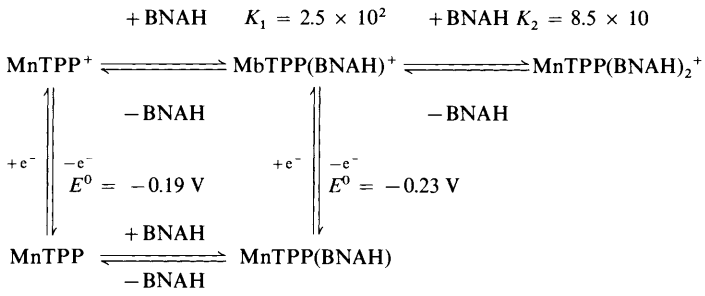

Scheme 2.

ratio, which indicates that the BNAH ligand exchanges rapidly with ZnTPP on the n.m.r. time scale. The $\delta_f - \delta$ value of each proton resonance of BNAH increases with an increase in the ZnTPP ratio, reaching a constant value in the region of high ratio of ZnTPP to BNAH (>2), where the ratio of the complexes BNAH to free BNAH becomes a constant value which is determined by the initial concentration of ZnTPP (2.93×10^{-2} mol dm^{-3}) and the K value. The magnitude of the shifts of the BNAH signals by the complex formation with ZnTPP is in the order NH_2 > 2-CH ≫ 4-CH ≫ Ph > NCH_2 > 5-CH > 6-CH [Figure 5(*a*)]. The observed upfield chemical shifts may be induced by the porphyrin ring current, which causes the larger shifts ($\delta_f - \delta$) with the smaller distances and the larger angle between a proton of the BNAH ligand and the centre of the porphyrin ring.[25] Thus, the observed order of the $\delta_f - \delta$ value suggests that the co-ordination site is the carbonyl oxygen of BNAH, where the distances of NH_2 and 2-CH protons from the centre of the porphyrin ring are expected to be smaller than those of other protons, although the exact orientation of the bound $COCNH_2$ group with respect to the dihydropyridine ring is unknown.

An NADH model compound BNAH also forms a 1:1 complex with Zn^{2+} ion without a porphyrin ligand. The absorption spectrum of BNAH (λ_{max} 350 nm) is red-shifted with an isosbestic point by the addition of $Zn(ClO_4)\cdot 6H_2O$ to a MeCN solution of BNAH. The K_1 value for the Zn^{2+}–BNAH complex ($K_1 = 1.2 \times 10^4$ dm^3 mol^{-1}), determined by the plot based on equation (3), was much larger than that of the ZnTPP–BNAH complex (Table 1). The ^{1}H n.m.r. signal of NH_2 protons of BNAH is shifted to slightly lower field by the interaction between the carbonyl oxygen of BNAH and Zn^{2+} ion, as shown in Figure 5(*b*).

Spin States of the Complexes Formed between $FeTPP^+$ *and* BNAH.—The ^{1}H n.m.r. signals of pyrrole protons of iron(III) porphyrin complexes are known to be quite sensitive to the spin states; pyrrole signals in the δ 70–80 and –15 region are characteristic for high-spin[26] and low-spin[27] species, respectively. The pyrrole proton signals of $FeTPPClO_4$ which has an admixed S 3/2, 5/2 spin-state appeared at δ 5–26 in CD_2Cl_2.[28] Addition of one and two mol equiv. of BNAH to a CD_2Cl_2 solution of $FeTPPClO_4$ (2.0×10^{-2} mol dm^{-3}) to form mainly $FeTPP(BNAH)^+$ and $FeTPP(BNAH)_2^+$, respectively, resulted in a significant downfield shift of the pyrrole proton signal in the δ 70–80 (high spin) region. Approximate Curie–Law behaviour is observed for the pyrrole proton and the *meta*-phenyl proton resonances of $FeTPP(BNAH)^+$ and $FeTPP(BNAH)_2^+$, which indicates that no spin admixture may be involved between S 3/2 and 5/2.[9] Thus, these two BNAH complexes could be simple high-spin paramagnetic molecules with S 5/2. The *meta*-phenyl proton resonance of $FeTPPClO_4$ in the presence of one mol equiv. of BNAH is different from that in the presence of two mol equiv. of BNAH, and a single averaged resonance was observed at the in-between region where the ratio of BNAH to $FeTPPClO_4$ was changed between one and two, indicating that the ligand exchange between $FeTPP(BNAH)^+$ and $FeTPP(BNAH)_2^+$ is fast on the n.m.r. time scale.

It should be noted that formation of such a six-co-ordinate high-spin iron(III) porphyrin complex $FeTPP(BNAH)_2^+$ is unusual, since most synthetic high-spin iron(III) porphyrin complexes are known to be five-co-ordinate,[26] although six-co-ordinate high-spin complexes are often observed in naturally occurring systems such as methaemoglobin and metmyoglobin.[29,30] The high-spin state of $FeTPP(BNAH)_2^+$ (9.8×10^{-3} mol dm^{-3}) was further confirmed by the e.s.r. spectrum at 77 K, which showed the characteristic anisotropic signals at $g_\perp = 5.7$ and $g_\parallel = 2.0$, as expected for high-spin iron(III) species.[31] The measurements of the solution magnetic susceptibilities using the Evans n.m.r. method also support the formation of the high-spin iron(III) species. The effective magnetic moments μ_{eff} in CD_2Cl_2 were found to be 5.9 μ_B* at 233 K and 5.6 μ_B at 296 K for $FeTPP(BNAH)^+$ and 6.0 μ_B at 233 K for $FeTPP\text{-}BNAH)_2^+$, both of which agree well with the calculated value of 5.92 μ_B for a pure S 5/2 state. The μ_B value of $FeTPP\text{–}(BNAH)_2^+$ in the presence of a large excess of BNAH at 296 K decreases gradually with time due to the occurrence of slow reduction in the next section.

Oxidation of BNAH *by* $FETPP^+$.—Sluggish oxidation of BNAH by $FeTPPClO_4$ occurred in both the absence and presence of oxygen in CH_2Cl_2. When the solvent CH_2Cl_2 was replaced by an aprotic polar solvent MeCN, BNAH was readily oxidized by $FeTPPClO_4$ in the absence of oxygen to yield BNA^+. In this case, however, the reduced product was not FeTPP and at present it has not been identified. When the oxidation of BNAH by $FeTPPClO_4$ was carried out in MeCN under an atmospheric pressure of oxygen, BNA^+ and μ-oxo dimer $(FeTPP)_2$ are formed as shown in Figure 6(*a*). The stoicheiometry of the reaction [equation (14)] has been

$$BNAH + 2\,FeTPP^+ + \tfrac{1}{2}O_2 \longrightarrow BNA^+ + (FeTPP)_2O + H^+ \quad (14)$$

determined from the spectroscopic titration as shown in Figure 6(*b*), which shows BNAH is oxidized by 2 mol equiv. of $FeTPPClO_4$ in MeCN. The quantitative formation of BNA^+ and $(FeTPP)_2O$ were confirmed by the ^{1}H n.m.r. and the visible spectra, respectively, and the release of the equivalent amount of protons [equation (14)] was confirmed by the pH analysis of the product (see the Experimental section). Since FeTPP is known to be oxidized by oxygen to yield the μ-oxo-dimer,[32] the oxidation of BNAH may be by two mol equiv. of $FeTPP^+$ in the

* 1 $\mu_B = 9.274\,02 \times 10^{-23}$ J T^{-1}.

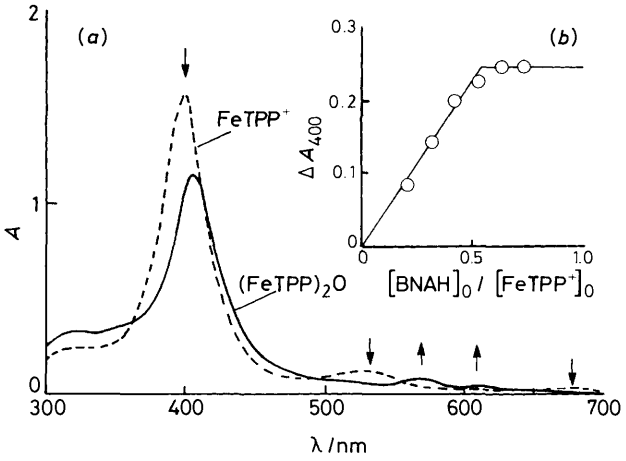

Figure 6. (*a*) Visible spectroscopic change in the reaction of $FeTPPClO_4$ (1.1×10^{-5} mol dm^{-3}) with BNAH (1.2×10^{-5} mol dm^{-3}) in the presence of oxygen in MeCN; the broken and solid lines show the spectra before and after the reaction, respectively. (*b*) Plot of the change in the absorbance at 400 nm for the reaction of $FeTPPClO_4$ (8.4×10^{-6} mol dm^{-3}) with BNAH in the presence of oxygen in MeCN as a function of the ratio of the initial concentration of BNAH to $FeTPPClO_4$, $[BNAH]_0/[FeTPP^+]_0$.

When BNAH was replaced by [4-^{2}H]BNAH, the deuterium isotope effect ($Y_H/Y_D = 1.7 \pm 0.1$) was observed in the oxidized product, BNA^+ (see the Experimental). Thus, the two-electron oxidation of BNAH by $FeTPP^+$ [equation (15)] may proceed *via* the intramolecular electron transfer from BNAH to $FeTPP^+$ in the $FeTPP(BNAH)^+$ complex, followed by proton transfer from $BNAH^{+\bullet}$ to FeTPP or MeCN to give BNA$^\bullet$ radical, and the second facile electron transfer from BNA$^\bullet$ to $FeTPP^+$ yields the product, BNA^+, Scheme 3. The observed deuterium isotope effects is thus ascribed to the deprotonation of $BNAH^{+\bullet}$. It may be interesting to note that the magnitude of the isotope effect ($Y_H/Y_D = 1.7$) is the same as the value of the primary kinetic isotope effect for the proton transfer from $BNAH^{+\bullet}$ to pyridine ($k_H/k_D = 1.7$)[33] and that the pK value of the protonated pyridine (pK 5.3) is similar to that of a protonated porphyrin (pK 4.4 for H_3TPP).[34]

The rate of formation of $(FeTPP)_2O$ is the same as the rate of decay of $FeTPP^+$ as shown in Figure 7, and it obeyed pseudo-first-order kinetics. Thus, the oxidation of BNAH by $FeTPP^+$ [equation (15)] may be the rate-determining step which is followed by the formation of $(FeTPP)_2O$ [equation (16)]. The pseudo-first-order rate constants k_{obs} of various BNAH derivatives (X-BNAH) are constant with respect to the change of the X-BNAH concentrations, as shown in Figure 8, where the

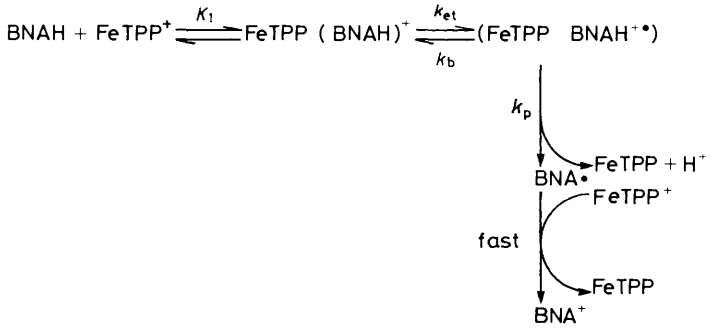

Scheme 3.

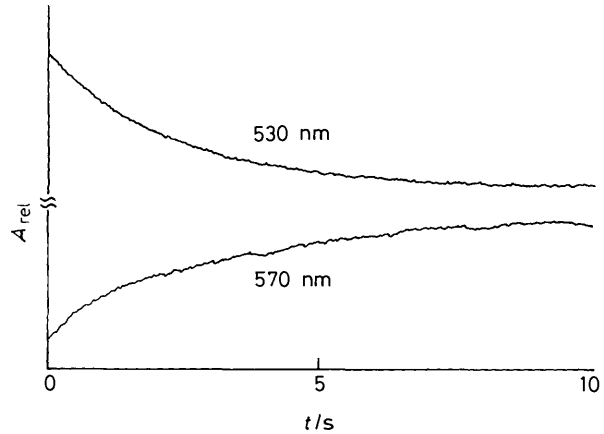

Figure 7. Kinetic curves of the decay of $FeTPPClO_4$ (530 nm) and the formation of $(FeTPP)_2O$ (570 nm) for the oxidation of BNAH by $FeTPPClO_4$ under a four times atmospheric pressure of oxygen in MeCN at 298 K.

presence of oxygen [equation (15)], followed by the oxidation of the resulting FeTPP by oxygen [equation (16)].

$$BNAH + 2\,FeTPP^+ \longrightarrow BNA^+ + H^+ + 2\,FeTPP \quad (15)$$

$$2\,FeTPP + \tfrac{1}{2}\,O_2 \longrightarrow (FeTPP)_2O \quad (16)$$

k_{obs} value of X-BNAH increases with an increase in the electron-donating ability of the substituent X. According to Scheme 3, k_{obs} may be given by equation (17), where k_{et} and k_b are the

$$k_{obs} = k_{et}k_pK_1[BNAH]_0/[(k_b + k_p)(1 + K_1[BNAH]_0)] \quad (17)$$

rate constants of forward and backward electron transfer, respectively, between BNAH to $FeTPP^+$ in the $FeTPP(BNAH)^+$ complex; k_p is the rate constant of the deprotonation of $BNAH^{+\bullet}$; K_1 is the formation constant of $FeTPPBNAH)^+$ [equation (1)]. When $K_1[BNAH] \gg 1$, equation (17) is reduced to equation (18). According to equation (18), k_{obs} is constant

$$k_{obs} = k_{et}k_p/(k_b + k_p) \quad (18)$$

with the change of the BNAH concentration, in accordance with the observation in Figure 8.

A more quantitative discussion can be achieved by comparing the observed rates with the calculated electron-transfer rate constants using the Marcus theory for the rates of outer-sphere electron-transfer reactions.[35] The Marcus relation for the rate constant of the electron transfer from the reductant (1) to the oxidant (2), k_{12}, is given by equation (19),[35] where k_{11} and k_{22} are the rate constants of the corresponding self-

$$k_{12} = (k_{11}k_{22}K_{12}f)^{\frac{1}{2}} \quad (19)$$

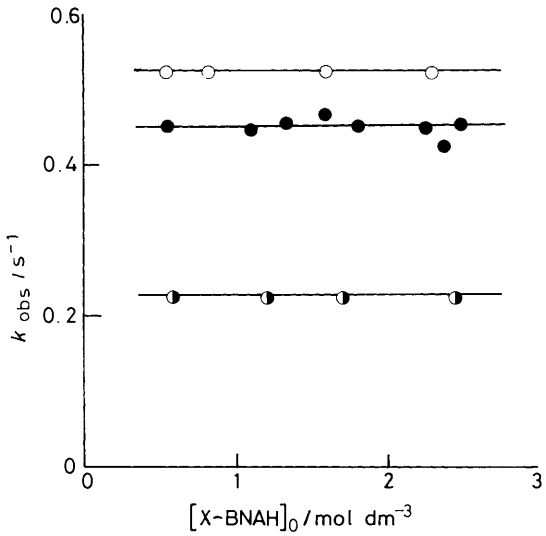

Figure 8. Plots of the observed pseudo-first-order rate constants (k_{obs}) *vs.* the concentration of NADH model compounds, 4-MeOBNAH (○), BNAH (●), and 2,4-Cl_2BNAH (◑), for the oxidation of NADH model compounds by $FeTPPClO_4$ (0.56–1.5/10^4 mol dm^{-3}) in the presence of oxygen in MeCN at 298 K.

Table 2. Comparison of the observed first-order rate constants (k_{obs}) for the oxidation of NADH model compounds (X-BNAH) by $FeTPP^+$ in the presence of oxygen with the calculated rate constants (k_{et}) for the intramolecular electron transfer from X-BNAH to $FeTPP^+$ in the $FeTPP(X\text{-}BNAH)^+$ complex in MeCN at 298 K.

X-BNAH	k_{obs}[a]/s^{-1}	k_{et}[b]/s^{-1}
4-MeOBNAH	0.52	4.0
BNAH	0.45	0.7
2,4-Cl_2BNAH	0.23	0.5

[a] The experimental errors are within ±10%. [b] Obtained from the calculated second-order rate constants of the electron transfer (k_{12}) and the formation constant K_1 (Table 1); for the calculation of k_{12}, see the text.

exchanges and K_{12} is the equilibrium constant for the electron-transfer reaction and the parameter f is given by equation (20),

$$\log f = (\log K_{12})^2/[4 \log (k_{11}k_{22}/Z^2)] \quad (20)$$

where Z, the frequency factor, is taken as 10^{11} dm^3 mol^{-1} s^{-1}.[35] The K_{12} value is obtained from the oxidation potential of X-BNAH (E^0_{ox}) and the reduction potential of $FeTPP^+$ (E^0_{red}) by using equation (21). Then, the rate constant of electron transfer

$$\log K_{12} = (-F/2.3RT)(E^0_{ox} - E^0_{red}) \quad (21)$$

from X-BNAH to $FeTPP^+$ (k_{12}) can be calculated from the reported values of self-exchange rate constants for X-BNAH (1×10^9 dm^3 mol^{-1} s^{-1})[10] and $FeTPP^+$ (1×10^9 dm^3 mol^{-1} s^{-1})[36] and the redox potentials of X-BNAH (Table 1)[10] and $FeTPP^+$ (0.14 V *vs.* SCE) by using equations (19)–(21). In order to compare between the calculated and observed values, the second-order rate constants (k_{12}) should be corrected to the corresponding first-order rate constants $k_{12}K_1^{-1}$ which correspond to the intramolecular electron-transfer rate constants (k_{et}). Although the K_1 values in MeCN are not known, they are assumed to be the same as those in CH_2Cl_2 (Table 1). The calculated intramolecular electron-transfer rate constants (k_{et}) are listed in Table 2, together with the observed rate constants (k_{obs}). As seen in Table 2, the observed first-order rate constants (k_{obs}) are somewhat smaller than the calculated electron-transfer rate constants (k_{et}) as expected from equation (18).

The mechanistic involvement of the $FeTPP(BNAH)^+$ complex may be alternatively expressed by equation (22), where the

$$FeTPP(BNAH)^+ \overset{K_1^{-1}}{\rightleftharpoons} BNAH + FeTPP^+ \underset{k'_b}{\overset{k'_{et}}{\rightleftharpoons}} (BNAH^{+\bullet}\ FeTPP) \quad (22)$$

$FeTPP(BNAH)^+$ complex does not lie along the reaction pathway, and does not take part in the equilibrium. The reactions subsequent to the electron transfer from BNAH to $FeTPP^+$ [equation (22)] are the same as those in Scheme 1. In this case, the observed first-order rate constant (k_{obs}) is expressed by equation (23) instead of equation (18). However, equation (23) is kinetically equivalent to equation (18), and they are indistinguishable from each other. Essentially the same discussion on the comparison between the observed and calculated rate constants, described above, is applied to equation (23), when the calculated rate constant corresponds

$$k_{obs} = k'_{et}k_p/[K_1(k'_b + k_p)] \quad (23)$$

to k'_{et} which should be compared with $k_{obs}K_1$. In any case, it can be concluded that the rates of two-electron oxidation of X-BNAH by $FeTPP^+$ together with the competition between the back electron transfer from FeTPP to $X\text{-}BNAH^{+\bullet}$ and the deprotonation of $X\text{-}BNAH^{+\bullet}$.

Acknowledgements

This work was supported by the Takeda Science Foundation.

References

1 B. Alberts, D. Bray, J. Lewis, M. Raff, K. Roberts, and J. D. Watson, 'Molecular Biology of the Cell,' Garland, New York, 1983, ch. 9; L. Stryer, 'Biochemistry,' Freeman, 1988, New York. ch. 17.
2 Y. Hatefi, *Ann. Rev. Biochem.*, 1985, **54**, 1015; I. E. Hassinen, *Biochim. Biophys. Acta*, 1986, **853**, 135.
3 A. J. Paine, 'Essays in Biochemistry,' ed. P. N. Campbell and R. D. Marshall, Academic Press, London, 1981, vol. 17, p. 85; R. E. White and M. J. Coon, *Ann. Rev. Biochem.*, 1980, **49**, 315; E. P. Guengerich and T. L. MacDonald, *Acc. Chem. Res.*, 1984, **17**, 9.
4 H. Eklund and C.-I. Brändén, 'Zinc Enzymes,' ed. T. G. Spiro, Wiley-Interscience, New York, 1983, ch. 4.
5 D. J. Creighton and D. S. Sigman, *J. Am. Chem. Soc.*, 1971, **93**, 6314; D. J. Creighton, J. Hajdu, and D. S. Sigman, *ibid.*, 1976, **98**, 4619; A. Ohno, H. Yamamoto, and S. Oka, *ibid.*, 1981, **103**, 2041; R. A. Gase and U. K. Pandit, *ibid.*, 1979, **101**, 7059; S. Fukuzumi, N, Nishizawa, and T. Tanaka, *J. Chem. Soc., Perkin Trans. 2*, 1985, 371.
6 J. W. Buchler, 'Porphyrins and Metalloporphyrins,' ed. K. M. Smith, Elsevier, New York, 1975, p. 157.
7 R. Quinn, M. Nappa, and J. S. Valentine, *J. Am. Chem. Soc.*, 1982, **104**, 2588; V. L. Balke, F. A. Walker, and J. T. West, *ibid.*, 1985, **107**, 1226; K. M. Kadish and C. H. Su, *ibid.*, 1983, **105**, 177; D. Lavalette, C. Tetreau, and M. Momenteau, *ibid.*, 1979, **101**, 5395; F. A. Walker, M.-W. Lo, and M. T. Ree, *ibid.*, 1976, **98**, 5552; G. N. La Mar and F. A. Walker, *ibid.*, 1973, **95**, 1782.
8 M. Nappa and J. S. Valentine, *J. Am. Chem. Soc.*, 1978, **100**, 5075; S. J. Cole, G. C. Curthoys, E. A. Magnusson, and J. N. Phillips, *Inorg. Chem.*, 1972, **11**, 1024; C. H. Kirksey, W. P. Hambright, and C. B. Storm, *ibid.*, 1969, **8**, 2141.
9 S. Fukuzumi, Y. Kondo, and T. Tanaka, *J. Chem. Soc., Chem. Commun.*, 1985, 1053.
10 S. Fukuzumi, S. Koumitsu, K. Hironaka, and T. Tanaka, *J. Am. Chem. Soc.*, 1987, **109**, 305.
11 S. Fukuzumi, N. Nishizawa, and T. Tanaka, *J. Org. Chem.*, 1984, **49**, 3571.
12 E. B. Fleischer, J. M. Palmer, T. S. Srivastava, and A. Chatterjee, *J. Am. Chem. Soc.*, 1971, **93**, 3162.

13 P. Rothemund and A. R. Menotti, *J. Am. Chem. Soc.*, 1948, **70**, 1808.
14 A. Shirazi and H. M. Goff, *Inorg. Chem.*, 1982, **21**, 3420; A. D. Adler, F. R. Longo, and V. Varadi, *Inorg. Synth.*, 1976, **16**, 213.
15 T. Sakurai, K. Yamamoto, H. Naito, and N. Nakamoto, *Bull. Chem. Soc. Jpn.*, 1976, **49**, 3042.
16 C. A. Reed, T. Mashiko, S. P. Bentley, M. E. Kastner, W. R. Scheidt, K. Spartalian, and G. Lang, *J. Am. Chem. Soc.*, 1979, **101**, 2948.
17 W. B. Fleischer and T. S. Srivastava, *J. Am. Chem. Soc.*, 1969, **91**, 2403.
18 D. F. Evans, *J. Chem. Soc.*, 1959, 2003.
19 S. S. Eaton and G. R. Eaton, *Inorg. Chem.*, 1980, **19**, 1095.
20 E. S. Hanson, *Ind. Eng. Chem.*, 1949, **41**, 99; D. Ostfeld and I. A. Cohen, *J. Chem. Educ.*, 1972, **49**, 829.
21 J. R. Miller and G. D. Dorough, *J. Am. Chem. Soc.*, 1952, **74**, 3977; D. Gust and D. N. Neal, *J. Chem. Soc., Chem. Commun.*, 1978, 681; G. C. Vogel and J. R. Stahlbush, *Inorg. Chem.*, 1977, **16**, 950; E. F. Caldin and J. P. Field, *J. Chem. Soc., Faraday Trans. 1*, 1982, **78**, 1923.
22 O. W. Kolling, *Inorg. Chem.*, 1979, **18**, 1175.
23 K. M. Kadish and L. A. Bottomley, *Inorg. Chem.*, 1980, **19**, 832.
24 K. M. Kadish, L. A. Bottomley, and D. Beroiz, *Inorg. Chem.*, 1978, **17**, 1124; K. M. Kadish and S. Kelly, *ibid.*, 1979, **18**, 2968.
25 C. B. Storm, A. H. Turner, and M. B. Swann, *Inorg. Chem.*, 1984, **23**, 2743.
26 D. V. Behere and H. M. Goff, *J. Am. Chem. Soc.*, 1984, **106**, 4945; D. V. Behere, R. Birdy, and S. Mitra, *Inorg. Chem.*, 1982, **21**, 386; G. N. La Mar, G. R. Eaton, R. H. Holm, and F. A. Walker, *J. Am. Chem. Soc.*, 1973, **95**, 63; M. Zobrist and G. L. La Mar, *ibid.*, 1978, **100**, 1945; W. R. Scheidt, Y. J. Lee, D. K. Geiger, K. Taylor, and K. Hatano, *ibid.*, 1982, **104**, 3367.
27 G. N. La Mar and F. A. Walker, *J. Am. Chem. Soc.*, 1973, **95**, 1782; D. M. Collins, R. Countryman, and J. L. Hoard, *ibid.*, 1972, **94**, 2066; D. Lexa, J. Mispelter, and J.-M. Saveant, *ibid.*, 1981, **103**, 6806; P. R. Ortiz de Montellano, K. L. Kunze, and O. Augusto, *ibid.*, 1982, **104**, 3545; J. D. Satterlee, G. N. La Mar, and J. W. Frye, *ibid.*, 1976, **98**, 7275.
28 H. Goff and E. Shimomura, *J. Am. Chem. Soc.*, 1980, **102**, 31; A. D. Boersma and H. M. Goff, *ibid.*, 1982, **21**, 581; G. E. Toney, L. W. terHaar, J. E. Savrin, A. Gold, W. E. Hatfield, and R. Sangaiah, *Inorg. Chem.*, 1984, **23**, 2561.
29 E. Antonini and M. Brunori, 'Hemoglobin and Myoglobin in Their Reactions with Ligands,' North–Holland, Amsterdam, 1971.
30 R. Lemberg and J. Borrett, 'Cytochromes,' Academic Press, New York, 1973.
31 R.-J. Cheng, L. Latos-Grazynski, and A. L. Balch, *Inorg. Chem.*, 1982, **21**, 2412; J. Peisach, W. E. Blumberg, S. Ogawa, E. A. Rachmilewitz, and R. Oltzik, *J. Biol Chem.*, 1971, **246**, 3342; D. V. Behere and S. Mitra, *Inorg. Chem.*, 1979, **18**, 1723; W. R. Scheidt, I. A. Cohen, and M. E. Kastner, *Biochemistry*, 1979, **18**, 3546.
32 L. Latos-Grazynski, R.-J. Cheng, G. N. La Mar, and A. L. Balch, *J. J. Am. Chem. Soc.*, 1982, **104**, 5992; R. M. Richman and M. W. Peterson, *ibid.*, 1982, **104**, 5795; J. P. Collman, *Acc. Chem. Res.*, 1977, **10**, 265.
33 S. Fukuzumi, Y. Kondo, and T. Tanaka, *J. Chem. Soc., Perkin Trans. 2*, 1984, 673.
34 D. K. Lavallee and A. K. Gebala, *Inorg. Chem.*, 1974, **13**, 2004.
35 R. A. Marcus, *J. Phys. Chem.*, 1963, **67**, 853; *Ann. Rev. Phys. Chem.*, 1964, **15**, 155.
36 R. F. Pasternack and E. G. Spiro, *J. Am. Chem. Soc.*, 1978, **100**, 968.

Received 25*th July* 1988; *Paper* 8/03032D